Computational Mechanics 20 (1997) 164–169 © Springer-Verlag 1997

A comparative investigation of micro-flaw models for the simulation of brittle fracture in rock

E. Sellers, J. Napier

Abstract The search for a numerical method to model fracture formation around deep level gold mine excavations had led to the development of the DIGS (Discontinuity Interaction and Growth Simulation) boundary element code to simulate the incremental growth of fractures. However, the need to develop constitutive models of basic failure processes resulted in the adoption of a tessellation approach to simulate grain interaction and breakage. Linear variation displacement discontinuity elements are arranged in structures which simulate the microstructure of the rock by applying either a Voronoi (polygonal) or Delaunay (triangular) tessellation procedure.

The tessellation approach has been applied to investigate the role of micromechanical mechanisms such as preexisting pores and sliding flaws on the macroscopic failure patterns at a scale that is representative of realistic rock microstructures.

Procedures for calculating the crack density tensors and the average stress and strain in a sample permit comparison of the results with alternative models of brittle fracture such as continuum damage mechanics. Simulations of laboratory tests have revealed that the tessellation approach can represent experimentally observed macroscopic failure modes such as splitting in uniaxial compression and shear band formation in biaxial compression, as well as the dependence of strength and inelastic deformation on the flaw density.

1 Introduction

The proper analysis of energy change and deformation mechanisms in mining operations requires a basic understanding of the failure processes occurring in the rock surrounding the underground workings. This is necessary to distinguish between failure processes that are "slow" in the sense of occurring over a period of hours, days or longer and failure which occurs rapidly and which is associated with sudden fault slip or "bursting" of excavation walls or pillars. Enquiry into the nature of failure immediately demands an understanding of the rock fabric and the mechanisms controlling damage localization and rock disintegration. In addition to this, it is necessary to define the level of detail of the fundamental failure processes being studied. At the finest level interatomic breakage processes must be considered (Abraham et al. 1994; Marder and Gross 1995). In the present research it is recognized that rock is an inhomogeneous and particulate material and it is assumed that basic failure processes are controlled by stress distributions at the grain scale (millimetres or fractions of a millimetre). This implies that grain and matrix inhomogeneities, pre-existing cracks, pores and inclusions play a basic role in initiating macro fracture localizations in rock. The explicit treatment of all these processes is impractical and equivalent structures have to be devised to describe the basic material properties. Fracture growth is simulated by considering the interaction of randomly placed flaws and the sequential initiation of further fracturing from the basic flaw population. The approach is distinct from continuum treatments of failure and also admits concepts of randomness and "statistical mechanics" into the treatment of rock failure. This philosophical concept is more fruitful than an adherence to deterministic modelling practices.

It is also apparent that in order to reach the goal of describing macrofracture processes that occur in mining or other geotechnical applications, it is important to be able to synthesize explicit damage processes as equivalent continuum models. It is hoped that the present work will provide a means to construct damage models that can summarize efficiently, at a scale of metres or tens of metres, the finer level fracture behaviour.

Communicated by P. E. O'Donoghue, M. D. Gilchrist, K. B. Broberg, 6 January 1997

E. Sellers, J. Napier
Division of Mining Technology, CSIR,
P.O. Box 91230, Auckland Park, 2006, South Africa

Correspondence to: E. Sellers

This research has been sponsored by the Safety in Mines Research Advisory Committee (SIMRAC), under projects GAP029 and GAP332.

2 Numerical models for microfractures

To construct explicit models of interacting microcracks it is convenient to employ small strain dislocation densities to represent the cracks (Cleary 1976; Napier 1990). If it is further assumed that loading rates are sufficiently slow that elastodynamic stress waves do not play a significant role in the fracture growth processes, then the displacements and stresses induced by microcracks located on surfaces C (which are suitably smooth but not necessarily connected) are given by the following integral relationships:

$$u_k(P) = \int_C -\gamma_{ijk}(P,Q) D_i(Q) n_j(Q) \mathrm{d}S_Q \qquad (1)$$

$$\tau_{kl}(P) = \int_C -\Gamma_{ijkl}(P,Q) D_i(Q) n_j(Q) \mathrm{d}S_Q \qquad (2)$$

where P is the point of observation and where $D_i(Q) = u_i^-(Q) - u_i^+(Q)$ is the difference in the displacement vector components across the crack surface at point Q. The negative and positive superscripts denote, respectively, the sides of the surface opposite to the surface normal vector and on the same side as the surface normal $n_i(Q)$. Repeated indices in Eqs. (1) and (2) imply summation over the number of spatial dimensions of the problem. In isotropic elastic material, the influence kernels are given by

$$\gamma_{ijk} = \frac{1}{8\pi(1-\nu)} \left[\psi_{,ijk} - 2\nu\delta_{ij}\phi_{,k} - 2(1-\nu)(\delta_{jk}\phi_{,i} + \delta_{ik}\phi_{,j}) \right] \qquad (3)$$

$$\Gamma_{ijkl} = \frac{G}{4\pi(1-\nu)} \left[\psi_{,ijkl} - 2\nu(\delta_{kl}\phi_{,jj} + \delta_{ij}\phi_{,kl}) - (1-\nu)(\delta_{ik}\phi_{,jl} + \delta_{jk}\phi_{,il} + \delta_{il}\phi_{,jk} + \delta_{jl}\phi_{,ik}) \right] \qquad (4)$$

where, in two dimensions, $\psi = \frac{1}{2}(r^2 - r^2 \log r^2)$; $\phi = -\log r^2$ and $r = |P - Q|$. G is the shear modulus, ν is Poisson's ratio and δ_{ij} is the Kroneker delta. Commas in Eqs. (3) and (4) denote differentiation with respect to the co-ordinate components of point P (that is $\phi_{,ij} \equiv \partial^2\phi/\partial p_i \partial p_j$).

The numerical evaluation of Eqs. (1) and (2) requires that explicit shapes be assigned to the variation of the displacement discontinuity vector $D_i(Q)$ over fixed segments of the surface C, termed "elements". If the assigned shape has polynomial variation and if the element is flat, then the influence of each element can be evaluated analytically. For example, suppose that one such element is located between points $-b$ and b on the y-axis of a local co-ordinate system y-z. Let the discontinuity values over the domain $-b < y < b$ be given by

$$D_i(y) = \alpha_i + \beta_i y \qquad (5)$$

where subscript i refers to the components y or z.

By applying Eqs. (2) and (4), the normal stress component on the y-axis can be shown to be given by

$$\tau_{zz}(y,0) = \frac{G}{4\pi(1-\nu)} \left\{ 2(\alpha_z + y\beta_z) \left[\frac{1}{y+b} - \frac{1}{y-b} \right] + \beta_z \log\left(\frac{y+b}{y-b} \right)^2 \right\} \qquad (6)$$

It is apparent from Eq. (6) that near the ends of the element, $y = \pm b$, the stress values become singular. In particular, as $\varepsilon \to 0$, $\tau_{zz}(b-\varepsilon, 0) \to \infty$ and $\tau_{zz}(b+\varepsilon, 0) \to -\infty$ if $\alpha_z + b\beta_z > 0$ with similar behaviour at the other end of the element. Furthermore, it can be shown from Eq. (6) that $\int_{-b}^{b} \tau_{zz}(y,0)\mathrm{d}y$ is unbounded, precluding the computation of an average stress over the element. Equation (6) may still be usefully employed if suitable points $y = \pm c$ within the element are chosen where the representative boundary conditions are to be matched. This procedure allows stresses to be computed with reasonable accuracy away from the element extremities. It must be accepted that on the element itself, stresses may only be evaluated at the designated collocation points $y = \pm c$. Because of the singular behaviour of (6), the evaluation of geometrical configurations where elements are closely parallel (less than one fifth of the element length) or acutely angled (less than twenty degrees) cause numerical instability in the solution.

The simulation of microfracture processes is effected by specifying random assemblies of cracks which may be interconnected. For example, a given region of interest can be covered by a set of Voronoi polygons or Delaunay triangles (Napier and Peirce 1995). A subset of the edges of these polygons is selected and designated as pre-existing flaws with assigned strength an friction sliding properties. A specified load increment is applied and the mutual interaction (sliding or opening) between the existing cracks is solved by an iterative scheme. At this point stresses are evaluated at each collocation point within elements which are assigned to the, as yet, unmobilized cracks. Following this evaluation, one or more elements are selected for mobilization according to a postulated priority and the entire problem is re-solved. (For example, elements having a specified degree of overstress outside the defined strength could be selected). In this manner, successive growth increments are evaluated leading to the evolution of an overall pattern of fracturing. The solution at each stage is found by means of an accelerated Jacobi iterative scheme. This procedure offers certain advantages over distinct element methods in that explicit block lists are not required and crack surface contact conditions are easily resolved at each collocation point. No special treatment of detached regions has to be undertaken as it can be demonstrated that no stress is generated when C is a closed surface and $D_j(Q)$ represents a rigid body rotation or translation of the region inside C (Jaswon and Symm 1985).

3 Modelling of laboratory experiments

Numerical experiments in which a sequence of incremental displacements were applied to the surface of a rectangular block to simulate compression tests have been performed to study the fracture mechanisms induced in random Voronoi and Delaunay tessellation patterns (Napier and Peirce 1995; Napier et al. 1996). A distributed fracture pattern is observed in the case that all the overstressed elements are permitted to activate simultaneously. Application of an incremental, "weakest link" approach in which only the most favourable site is allowed to activate results in a fracture pattern which is initially similar to a shear band, but becomes distributed as loading progresses (Napier et al. 1996). In contrast, observations of compression test specimens suggest that microscopic fractures are initially randomly distributed (Krantz 1982). As the sample is compressed new microcracks form in the direction of maximum compression and finally combine into a macroscopic shear band (Hallbauer et al. 1973).

The results of triaxial compression tests (Stavropoulou 1979) and triaxial extension tests (Briggs and Vieler 1984) on quartzite rocks from the South African gold mines have demonstrated that the strength, deformation and failure

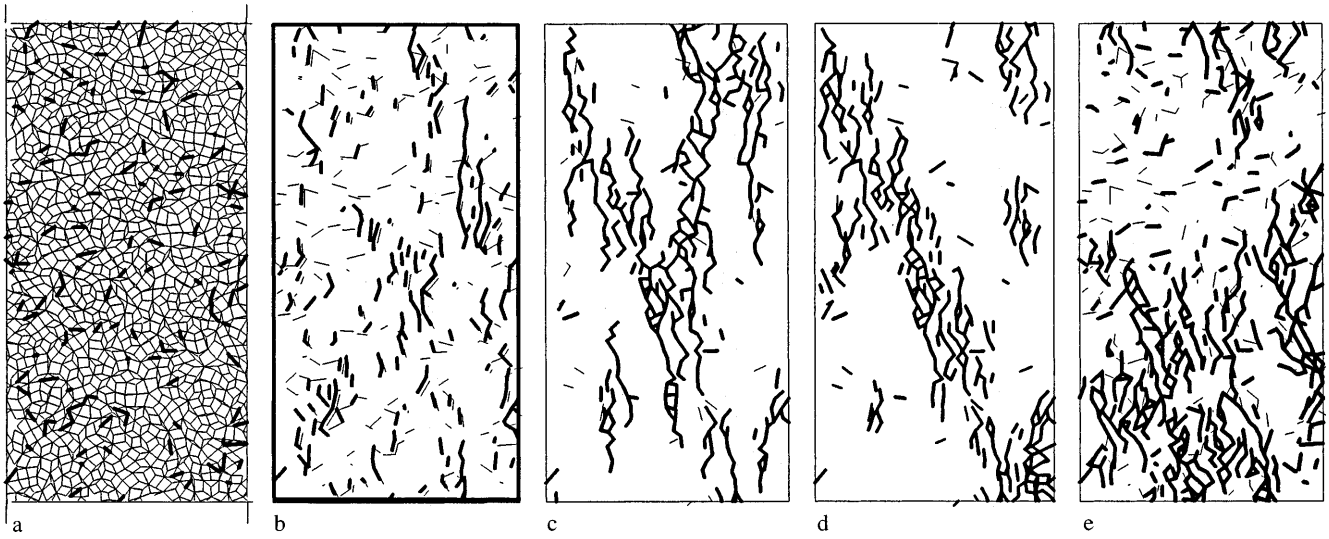

Fig. 1a–e. Typical fracture patterns in compression. **a** tesselation with flaws; **b** unconfined with 20% flaws; **c** unconfined with 4% flaws; **d** confined (10 MPa) with 4% flaws; **e** confined (50 Mpa) with 20% flaws

mode depends strongly on the ratio of quartz grains to matrix material. Thus, siliceous quartzites which contain more than 90% quartz, with welded grain boundaries, are stronger and more brittle than rocks which consist of quartz grains surrounded by weaker argillaceous matrix material. The tessellation procedure was therefore modified in an attempt to simulate a rock material consisting of quartz grains with some welded grain boundaries and other intergrain spaces filled with weaker, plastic, material. The objective was to determine if the fracture pattern and stress-strain response would depend on the flaws density.

The numerical "samples" are rectangles, 20 mm long and 10 m wide, and are tessellated with about 1000 Voronoi polygons, see for example Fig. 1a. The tests are analysed in plane strain conditions. A portion of the Voronoi grain boundaries are considered to be weaker material. The corners of the polygons are joined to the geometric centre of the polygon to provide intragranular fracture paths. A Mohr Coulomb strength criterion, with tensile cut-off, is specified on each potential fracture site. The properties are given in Table 1. The flaws and intergranular sites have a nonzero residual cohesion to simulate ductile flow and the intragranular sites have a higher initial cohesion which is reduced to zero on activation to simulate brittle fracture.

In the compression simulations, the sample is loaded by displacement increments applied to one end of the sample. In confined tests, the required confinement was applied as a stress boundary condition to the longer sides of the sample. In the extension tests, the sample was initially loaded to a "hydrostatic state" by applying 600 MPa stress in the axial and lateral directions. The axial stress was subsequently reduced in increments to simulate extension loading.

In an effort to compare the numerical experiments with physical experiments, a number of macroscopic measures such as the stress, the strain and the crack density have been formulated and are calculated during post processing of the DIGS results. The average strain $\langle \varepsilon_{ij} \rangle$ and the average stress $\langle \sigma_{ij} \rangle$ within the closed boundary Γ of a test specimen, of area A, can be determined from

$$\langle \varepsilon_{ij} \rangle = \frac{1}{2A} \int_{\Gamma} (u_i n_j + u_j n_i) \mathrm{d}\Gamma \text{ and}$$

$$\langle \sigma_{ij} \rangle = \frac{1}{A} \int_{\Gamma} (q_i \tau_{jk} n_k) \mathrm{d}\Gamma \tag{7}$$

where **u** is the displacement vector on Γ, **n** is the corresponding normal, the q_i are the co-ordinates of a point on Γ, and the τ_{jk} are the average stresses on Γ (Napier and Peirce 1995). The effective stress is the undamaged part of the material is given by

$$\langle \hat{\sigma}_{ij} \rangle = K^o_{ijkl} \langle \varepsilon_{kl} \rangle \tag{8}$$

where K^o_{ijkl} is the elastic stiffness tensor of the undamaged material (Lemaitre 1987). A measure of the average inelastic strain of k crack elements, in an area A, can be expressed as

$$\begin{aligned} \langle \varepsilon^i_{ij} \rangle &= \frac{1}{2A} \int_c (D_i n_j + D_j n_i) \mathrm{d}S \\ &= \frac{1}{2A} \sum_k (2 b_k (\overline{D}_i n_j + \overline{D}_j n_i)_k) \end{aligned} \tag{9}$$

Table 1. Constitutive properties specified for the different types of site

Site Type	Cohesion C_o (MPa)	Residual Cohesion C_m (MPa)	Friction angle ϕ	Residual friction ϕ_m/ψ_m	Dilation	Tension cutoff MPa
Intragrain	100	0	45°	30°	0	10
Intergrain	40	40	45°	30°	10°	10
Flaw	5	1	45°	30°	10°	1

where the integral is taken over the upper surface of all the cracks C (Horii and Yoshida 1994), and b_k is the half length and $\overline{D}_j$ the average displacement discontinuity on the kth element. A quantitative measure of the state of fracturing is obtained from the second order crack density tensor γ_{ij} which can be defined (Kachanov 1992), for k cracks in a region of representative area A by

$$\gamma_{ij} = \hat{\rho} \sum_k (b^2 n_i n_j)^{(k)} = \frac{1}{\sqrt{A}} \sum_k b^{(k)} \sum_k (b^2 n_i n_j)^{(k)} \quad (10)$$

where $\hat{\rho}$ defines the density of cracking (Napier and Peirce 1995).

The inelastic strain components given by Eq. (9) have been calculated on a 20×10 regular grid with a 1 mm spacing. The second invariant of the deviatoric part of the inelastic strain is

$$I2d = ((\langle \varepsilon^i_{11} \rangle - \langle \varepsilon^i_{22} \rangle)^2 + (\langle \varepsilon^i_{11} \rangle)^2 + (-\langle \varepsilon^i_{22} \rangle)^2)/6 + \langle \varepsilon^i_{12} \rangle^2 \quad (12)$$

and provides a measure of the shear deformation at a grid point and can indicate the positions of localized zones of deformation in the sample.

Typical fracture patterns for the biaxial compression tests are shown in Fig. 1. Each active flaw acts in a similar fashion to the sliding crack model (e.g. Horii and Nemat-Nasser 1986). Sliding on active flaws induces tensile stresses on some of the intragranular fractures. Activation of the most highly overstressed intragranular fracture leads to a further redistribution of stress and a sequence of fracturing is initiated. The ultimate fracture pattern depends on the density and the distribution of flaws and the confining pressure. In unconfined compression, as shown in Fig. 1b and 1c, the activated intragrain sites are generally aligned with the direction of maximum compression, suggesting an axial splitting mode of failure. Application of 10 MPa confinement to the sample with 4% flaws leads to a diagonal zone of en-echelon fractures, generally aligned with the maximum compression, as shown in Fig. 1d. Failure due to extensive en-echelon fracturing occurs in the sample with 20% flaws, confined to 50 MPa as shown in Fig. 1e. The fracture patterns compare well with patterns observed in plane strain tests on quartzite (Yumlu and Ozbay 1995).

The localised nature of deformation in a sample can be quantified by consideration of the corresponding contours of the second invariant of the deviatoric inelastic strain *I2d* in Fig. 2. The diagonal pattern of the regions of high *I2d* in Fig. 2a suggest that shear banding in will occur by linking of the vertical en-echelon fractures shown in Fig. 1b. In contrast, the sample with fewer flaws, see Fig. 1c and 2b, exhibited the axial splitting mode. The benefit of quantifying the localised deformation can be seen from Fig. 2c. The fracture pattern is outwardly similar to the unconfined case (compare Figs. 1c and 1d) and yet contours of *I2d* emphasise the diagonal shear band. Conjugate shear bands formed in the confined sample with 20% flaws as shown in Figs. 1e and 2d.

The fracture patterns induced in the triaxial extension tests are shown in Fig. 3. The cracks are initiated in tension due to stress concentrations from the sliding of flaws and are aligned in the direction of maximum compression. The failure patterns (e.g. Fig. 3a) are similar for all samples in which intragranular fracturing is permitted and compared well with the schematic diagram of fractures in a test on a 70% Quartzite specimen (Briggs and Vieler 1984) shown in Fig. 3b. The position of the final localized zone is confirmed by the contours of *I2d* given in Fig. 3c, and varies across the sample depending on the distribution of flaws, and the confinement as was observed in the experiments. The sample without intragrain fractures also exhibited fracturing in the direction of maximum compression, see

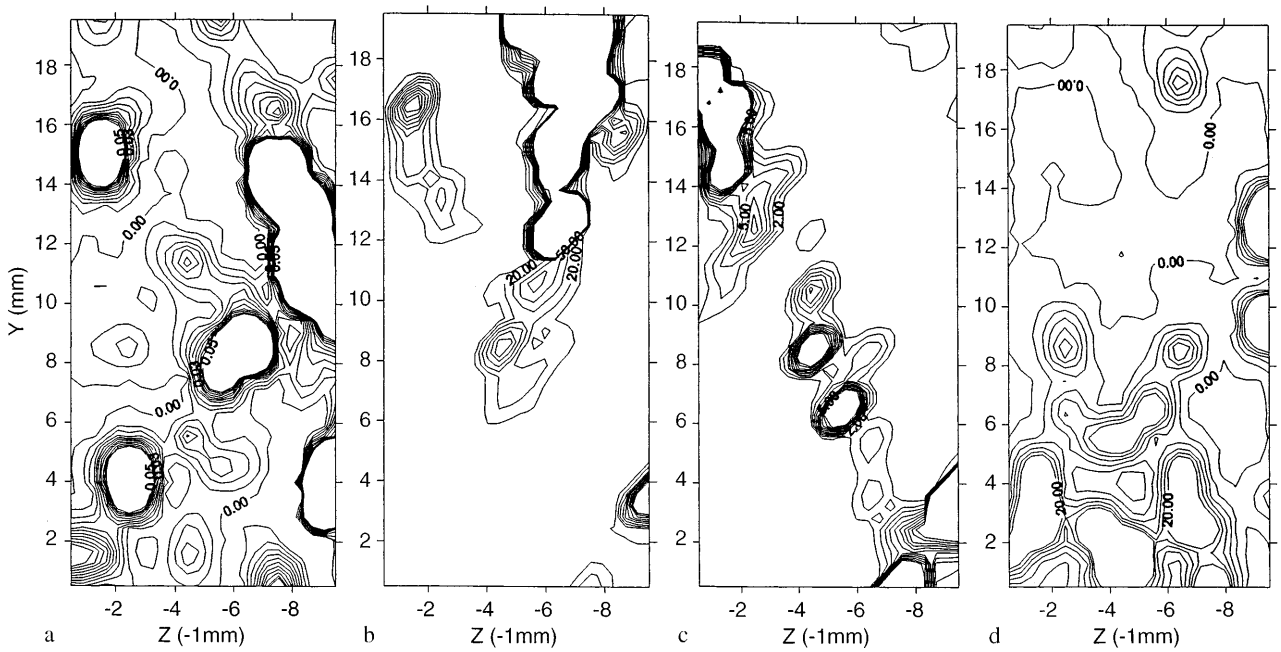

Fig. 2a–d. Typical contours of *I2d* of inelastic strain in compression. **a** unconfined with 20% flaws; **b** unconfined with 4% flaws; **c** confined (10MPa) with 4% flaws; **d** confined (50 Mpa) with 20% flaws

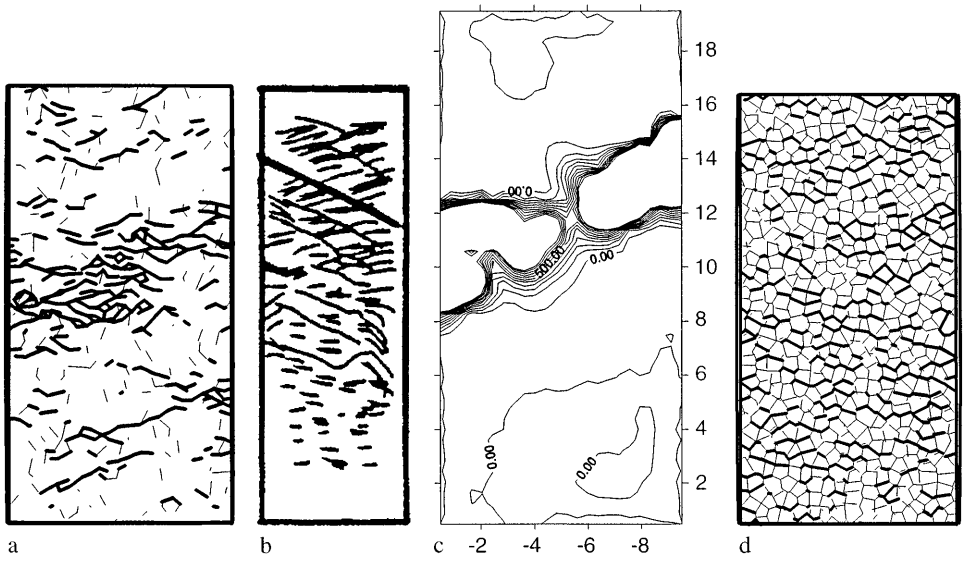

Fig. 3a–d. Typical extension results. **a** fracture pattern with 20% flaws; **b** observed pattern (Briggs and Vieler 1984). **c** contours of inelastic strain. **d** no intragranular fracturing permitted

Fig. 3d, and not the conjugate shear band formation observed in highly argillaceous rocks (Briggs and Vieler 1984). The contours of *I2d* indicate no strong localized zone.

The macroscopic stress–strain curves for the three uniaxial compression tests, obtained using Eq. (7), are given in Fig. 4a. At each displacement increment, prior to localisation, activation of fracturing results in non-linear hardening of the stress–strain response. The degree of nonlinearity depends on the density of flaws. The samples with intragranular fracturing exhibit softening once localisation is initiated which continues until the memory available in the computer becomes full or the analysis becomes numerically unstable. The sample with only intergrain fracturing exhibits the most nonlinearity and numerical instability occurs due to the rotation of polygons with completely fractured boundaries. A similar dependence of the strength and deformation on the density of flaws is shown in the stress strain response of the extension tests in Fig. 4b. A sample without flaws fails suddenly with a distributed fracture pattern due to sliding on the intragranular fractures when the stress state exceeds the Mohr Coulomb failure criterion.

Graphs of the stress–inelastic strain response for three uniaxial compression tests are shown in Fig. 5a and demonstrate that the majority of the deformation occurs in the lateral direction as observed in experiments (Stavropoulou 1979). The relationship between the crack pattern and the inelastic strain can be determined by comparing the angle of the principal direction of the crack density tensor γ_{ij} with those of the inelastic strain tensor $\langle \varepsilon_{ij}^{je} \rangle$, as shown in Fig. 5b for the sample with 20% flaws. The overall crack angle decreases with increasing axial strain whereas the principal directions of the inelastic strain remain constant. The intragrain fractures are shown to be directed within 1° of the loading axis and yet the direction of the principal inelastic strain is initially 12° and decreases with loading. This is because the crack density tensor takes no account of shear deformation (Kachanov 1990) and should not be used as a basis for modelling the damage in rock under compression (Kachanov 1982; Krajcinovic 1987).

In these simulations, the effective stress is only higher than the overall stress during the hardening portion of the stress–strain curve, see for example the case with 4% flaws in Fig. 4a. After softening has occurred, the effective stress is found to be lower than the overall stress. In addition, the

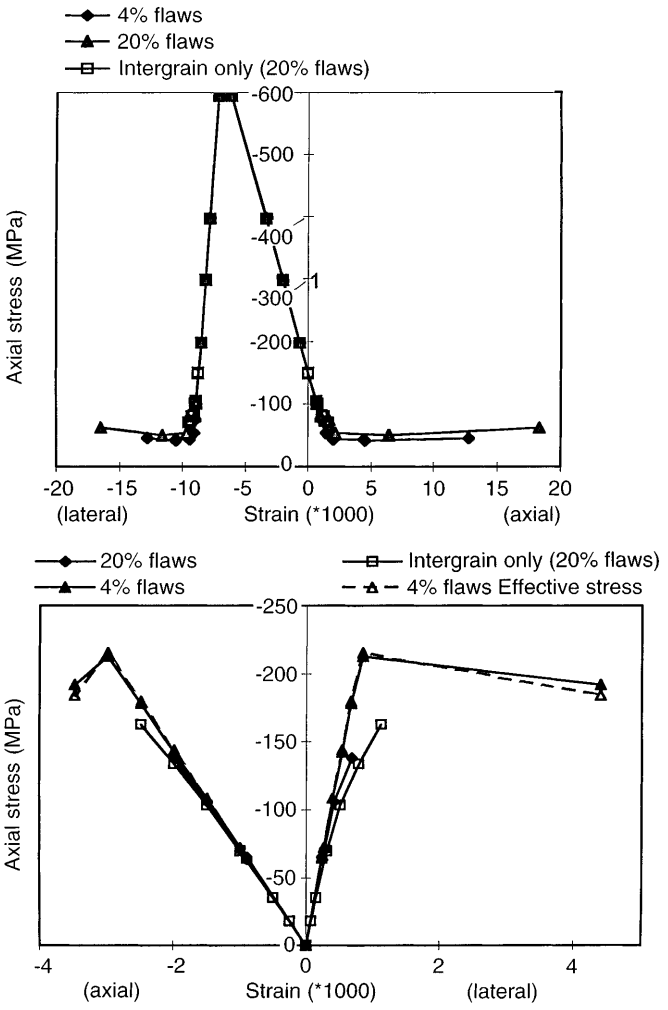

Fig. 4a,b. Average stress–average strain curves calculated for **a** extension and **b** compression tests

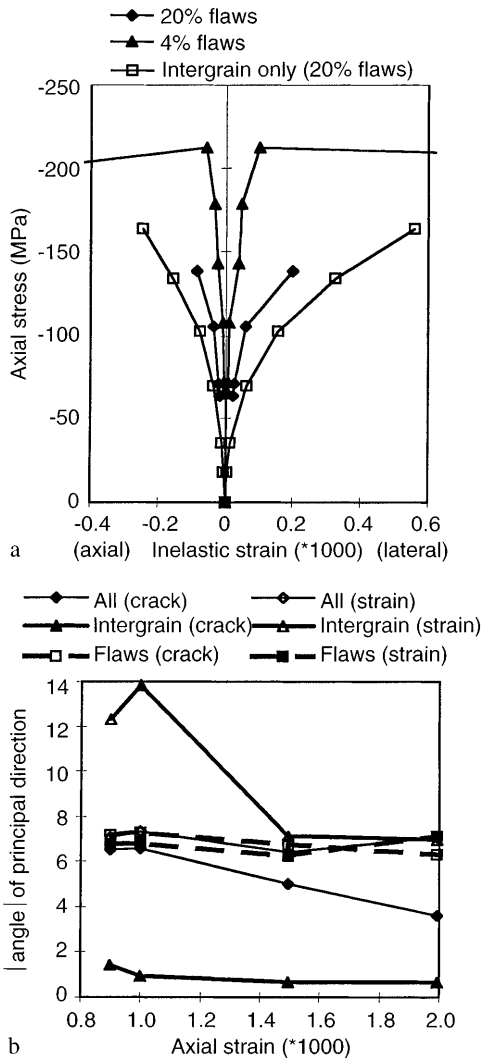

Fig. 5a,b. Investigation of effect of explicit damage with axial strain increase. **a** average stress–inelastic strain. **b** change of principal angle of inelastic strain

nonlinearity of effective stress–strain curves confirms doubts as to the applicability of the effective stress assumption in conventional continuum damage models (Krajcinovic 1987) under general states of stress (Baste and Audion 1991). Any damage model for rocks under compression should therefore combine the damage due to sliding on pre-existing flaws (Gambarrotta et al. 1992; Andriuex et al. 1986) and the opening of extension cracks (Kachanov 1982; Sellers 1994).

4 Conclusions

A tessellation approach has been developed for the modelling of rocks using the displacement discontinuity program DIGS. Sliding on pre-existing flaws induces a sequence of tensile failure events on intragranular fracture sites. Extension fracturing and localised failure under a state of compression, as observed in experiments, can be attributed to the internal stress rearrangements caused by the flaw deformation. An increase of the flaw density results in shorter, more evenly distributed cracks and thus the flaws can act both as fracture initiators and as barriers to extending cracks. Tessellations without intragranular sites cannot represent the observed failure along plastic slip lines, but could be suitable for concrete or sedimentary rocks such as sandstone which contain strong grains surrounded by a relatively weak matrix. The macroscopic material response is shown to be path dependent and exhibits stress induced anisotropy. Continuum approximations of such behaviour must consider the complex interactions between the deformation of flaws and weak grain boundaries and the formation of extension fractures within the stronger grains. Further research is required to calibrate the tessellations to represent particular types of rock in order to compare the development of the fracture zone around stopes in different geotechnical regions.

References

Abraham, F. F.; Brodbeck, D.; Rafey, R. A; Rudge, W. E. (1994): Instability dynamics of fracture: a computer investigation. Phys. Rev. Lett. 73, 272–275

Andriuex, S.; Bamberger, Y.; Marigo, J. (1986): Un modèle de matériau microfissuré pour les bétons et les roches. J. Theo. Appl. Mech. 5 471–513

Baste, S.; Audoin, B. (1991): On internal variables in anisotropic damage. Eur. J. Mech. A/Solids 10, 587–606

Briggs, D. J.; Vieler, J. D. S. (1984): Microfracture studies of quartzite in triaxial extension. COMRO (now Miningtek, CSIR, South Africa) Int. Res. Rep. 12/84

Cleary, M. P. (1976): Continuously distributed dislocation model for shear bands in softening materials. Int. J. Num. Meth. Eng. 10, 679–702

Gambarotta L.; Lagomarisino, S. (1993): A microcrack damage model for brittle materials. Int. J. Sol. Struct. 25, 803–833

Hallbauer, D. K.; Wagner, H.; Cook, N. G. W. (1973): Some observations concerning the microscopic and mechanical behaviour of quartzite specimens in stiff, triaxial compression tests. Int. J. Rock Mech. Min. Sci. 10, 713–726

Horii, H.; Nemat-Nasser, S. (1985): Compression-induced microcrack growth in brittle solids: axial splitting and shear failure. J. Geophys. Res. 90, 3105–3125

Jaswon M. A.; Symm, G. T. (1977): Integral methods in potential theory and elastostatics. Academic Press, London

Krajcinovic, D. (1989): Damage mechanics. Mech. Mat. 8, 117–197

Kranz, R. L. (1983): Microcracks in rocks: a review. Tectonophysics 100, 449–480

Lemaitre, J. (1987): Formulation and identification of damage kinetic constitutive equations. Cont. Dam. Mech., Springer-Verlag, Wien, 37–90

Napier, J. A. L. (1990): Modelling of fracturing near deep level mine excavations using a displacement discontinuity approach. In: Rossmanith, H.P. (ed.): Mechanics of jointed and faulted rock, Balkema, Rotterdam 709–715

Napier, J. A. L.; Peirce, A. P. (1995): Simulation of extensive fracture formation and interaction in brittle materials. In: Rossmanith, H.P. (ed.): Mechanics of Jointed and Faulted Rock-MJFR-2. Balkema, Rotterdam, 63–74

Napier, J. A. L.; Daehnke, A.; Hildyard, M. W.; Kuijpers, J. S.; Malan, D. F.; Sellers, E. J.; Turner, P. A. T. (1996): Quantification of stope fracture zone behaviour in deep level gold mines. J. SAIMM (in prep.)

Marder, M.; Gross, S. (1995): Origin of crack tip instabilities. J. Mech. Phys. Solids 43, 1–48

Sellers, E. J. (1994): An anisotropic damage model for rock. PhD. thesis, University of Cape Town

Stavropoulou, V. (1982): Constitutive laws for brittle rocks. PhD. Thesis, University of the Witwatersrand, Johannesburg

Yumlu, M.; Ozbay, M. U. (1995): A study of the behaviour of brittle rocks under plane strain and triaxial loading conditions. Int. J. Rock. Mech. Min. Sci. 32, 725–733